

Article

Location Scheme of Routine Nucleic Acid Testing Sites Based on Location-Allocation Models: A Case Study of Shenzhen City

Siwaner Wang^{1,2}, Qian Sun^{1,2}, Pengfei Chen^{1,2,*} , Hui Qiu^{1,2} and Yang Chen^{1,2}

¹ School of Geospatial Engineering and Science, Sun Yat-sen University, and Southern Marine Science and Engineering Guangdong Laboratory (Zhuhai), Zhuhai 519082, China

² Key Laboratory of Comprehensive Observation of Polar Environment (Sun Yat-sen University), Ministry of Education, Zhuhai 519082, China

* Correspondence: chenpf9@mail.sysu.edu.cn

Abstract: Since late 2019, the explosive outbreak of Coronavirus Disease 19 (COVID-19) has emerged as a global threat, necessitating a worldwide overhaul of public health systems. One critical strategy to prevent virus transmission and safeguard public health, involves deploying Nucleic Acid Testing (NAT) sites. Nevertheless, determining the optimal locations for public NAT sites presents a significant challenge, due to the varying number of sites required in different regions, and the substantial influences of population, the population heterogeneity, and daily dynamics, on the effectiveness of fixed location schemes. To address this issue, this study proposes a data-driven framework based on classical location-allocation models and bi-objective optimization models. The framework optimizes the number and location of NAT sites, while balancing various cost constraints and adapting to population dynamics during different periods of the day. The bi-objective optimization process utilizes the Knee point identification (KPI) algorithm, which is computationally efficient and does not require prior knowledge. A case study conducted in Shenzhen, China, demonstrates that the proposed framework provides a broader service coverage area and better accommodates residents' demands during different periods, compared to the actual layout of NAT sites in the city. The study's findings can facilitate the rapid planning of primary healthcare facilities, and promote the development of sustainable healthy cities.

Keywords: Corona Virus Disease 19 (COVID-19); Location-Allocation; Nucleic Acid Testing (NAT); Multi-Objective Optimisation Problem (MOOP)



Citation: Wang, S.; Sun, Q.; Chen, P.; Qiu, H.; Chen, Y. Location Scheme of Routine Nucleic Acid Testing Sites Based on Location-Allocation Models: A Case Study of Shenzhen City. *ISPRS Int. J. Geo-Inf.* **2023**, *12*, 152. <https://doi.org/10.3390/ijgi12040152>

Academic Editors: Baojie He, Deo Prasad, Ali Cheshmehzangi, Wu Deng, Samad Sepasgozar, Xiao Liu and Wolfgang Kainz

Received: 31 January 2023
Revised: 24 March 2023
Accepted: 3 April 2023
Published: 5 April 2023



Copyright: © 2023 by the authors. Licensee MDPI, Basel, Switzerland. This article is an open access article distributed under the terms and conditions of the Creative Commons Attribution (CC BY) license (<https://creativecommons.org/licenses/by/4.0/>).

1. Introduction

Infectious diseases pose a serious threat to global health security [1]. According to the World Health Organization (WHO), infectious diseases caused the deaths of nearly 20 million people in 2019, making up 36% of all fatalities worldwide [2]. Since the Corona Virus Disease 19 (COVID-19) first emerged at the end of 2019, it has caused a global epidemic that has led to more than 6.5 million fatalities thus far, and caused a significant depression in economic activity worldwide [2]. Despite the fact that COVID-19 is now less deadly, the virus remains a great risk to the public health system, given its high genetic variability and infectivity, which might cause a squeeze on medical resources, especially in densely populated areas.

Nucleic Acid Testing (NAT), as a gold standard means of virus diagnostic testing, is widely used worldwide to identify and take timely actions in respect of infectious people suffering from COVID-19 [3]. Compared to self-reported testing methods used in Western countries, city-wide NAT sites have been set up in China in order to provide flexible public testing services. However, because of China's massive and unevenly distributed population, the demand for NAT services could significantly vary within a specific region [4]. Existing healthcare facilities, including hospitals and clinics, cannot provide enough NAT service

to cover the entire population. To that end, additional NAT sites are commonly deployed in other public facilities, such as community centres, to increase service coverage. These public NAT sites were believed to primarily relieve the stress of the healthcare system and increase the coverage of the tested population, at a relatively low cost [4,5]. However, due to the enormous sizes of Chinese cities and unequal population distribution, determining the appropriate locations of NAT sites has emerged as a critical challenge in public health management [6].

The difficulty of siting public health facilities has been extensively studied in previous research. Existing methods can be roughly classified into two categories, that is, scoring-based and model-based methods. Scoring-based methods generally evaluate the suitability of each alternative facility from selected criteria, by incorporating environmental context and perceptions from experts or the public [7–9]. The main issues in scoring-based methods include the integration of each criterion score, and the identification of the optimization solution. For example, Ali et al. [7] selected 12 environmental and economic criteria to evaluate the alternative locations for sanitary landfill sites in Memari Municipality, India, in which the analytic hierarchy process (AHP) and fuzzy technique for order of preference by similarity to ideal solution (FTOPSIS), are subsequently applied to weight the selected criteria and identify the optimal solution. Similarly, Ajaj et al. [8] adopted six criteria to score alternative hospital sites, and applied AHP to produce a suitability map for guiding new hospital site selection. Although scoring-based methods can comprehensively evaluate the suitability of alternative sites, the effectiveness would highly rely on the selection of criteria, which might suffer from the subjectivity issue. Also, the criteria in score-based methods are usually designed for a specific case and region, limiting their transferability in practice.

In contrast, model-based methods generally solve the siting problem by breaking the problem into simpler sub-problems and trying to find the optimal solution under certain constraints, with the Location-Allocation (LA) approach being one of the most representative model-based methods in practice [10,11]. Different LA algorithms have been designed to solve the optimization of facility locations under varying constraints, such as travel cost or the number of facilities. For example, Devi et al. [12] developed an LA model for determining influenza testing laboratories in Maharashtra, India, using a bi-objective mixed integer programming method, in which a suitable siting solution was expected to ensure that: (1) people reached the facility as soon as possible; and (2) the total cost for running the clinics was minimal. Similar practices could be also observed in determining the running of isolated wards during the control of the 2009 H1N1 outbreak in China [13].

While the constraints differ in existing LA algorithms, the P-median, P-center, maximum coverage location problem (MCLP), and location set covering problem (LSCP) models, could be summarized as the four basic LA algorithms most commonly used in healthcare services planning [14–17]. The P-median, P-center, and MCLP models are all suitable for problems with a fixed facility number, whilst their optimisation objectives differ. The objective of the P-center model is to minimise the maximum travel distance between a single demand point and a facility point. In contrast, the P-median model aims to minimise the total travel cost between the demand point and the facility point [18]. The MCLP model is used to maximise the service area [19,20]. When the number of facilities points to deploy is unknown, the LSCP model can determine the minimum number of facilities, such that all demands within a designated service time or distance, would be met [16,21,22]. However, most LA model concerns in previous research of public health services have centred on the planning of new facilities based on the locations of existing service sites [23–25], while in the case of deploying NAT sites, none of the models mentioned above can solely deal with this problem, since both the number and distribution of NAT sites are unknown.

In this study, our primary goal is to design a set of candidate plans that simultaneously determine the number and distribution of NAT sites. In principle, the NAT service should be as equitably accessible to the public as possible [26]. Therefore, the candidate plans should minimize the total distance between demand points and facilities, ensuring the

highest level of overall accessibility within the area. For this purpose, we believe that the P-median model is more suitable for NAT site deployment than the P-center model and the MCLP model [27–29]. As the number of facilities is unknown, we apply the LSCP model to determine the number of NAT sites for each candidate plan under different tolerances of travel cost, before implementing the P-median model.

The second goal of our study is to select the optimal candidate plan. When deploying NAT sites, numerous factors need to be taken into consideration [30]. The cost of public travel to access NAT services generally decreases with the increasing number of sites. However, when new sites are required to improve the NAT service, construction costs must be carefully considered in order to minimize financial expenses [31]. Thus, the deployment of NAT sites can be viewed as a multi-objective optimization problem (MOOP) [32,33], where the accessibility and construction costs of NAT sites need to be strategically balanced.

MOOP algorithms, such as the weighted linear combination method and the analytic hierarchy process, have been used as a posteriori decision algorithm for LA models to determine the optimal number and location of distributions under multiple objectives [34–37]. However, these algorithms require the decision-maker to provide precise preferences, which is difficult in the NAT site location problems. Knee point identification (KPI) is a geometric-based tool for resolving the MOOP issue by finding the optimal option without prior knowledge [38,39], which would significantly reduce the subjectivity issue in solving MOOPs [40,41]. Traditional KPI methods include the convex hull of individual minima (CHIM) [42], minimum Manhattan distance (MMD) [43], and reflex angle [44]. CHIM determines the knee point as the point on the curve with the greatest distance to the plane of the extreme value, which has the disadvantage of limited applicability to convex curves, and neglecting Pareto-front edges [45]. MMD identifies knee point(s) by the minimum Manhattan distance from the hyperplane formed by the minimum [43]. Given that the abovementioned methods both operate on the same concept, the performance of CHIM is equivalent to that of MMD when there is just one knee point [46,47]. The angle-based reflex angle method is simple to calculate but concentrates on local information, which may lead to less accurate results [48]. To improve the accuracy of angle-based methods, Satopaa et al. proposed a general algorithm for discrete data called Kneedle, in conjunction with a mathematical definition based on the curvature of continuous functions [44]. Compared with other evolutionary algorithms, Kneedle not only maintains preference-free features, but also has high robustness, wide applicability, computational convenience, and intuitive results.

In summary, this study aims to develop a data-driven framework for the deployment of NAT sites that balances the accessibility of NAT services with construction costs. The framework integrates two Location-Allocation models, with a bi-objective multi-objective optimisation model to iteratively determine the optimal number and location of NAT sites. Firstly, the LSCP model is used to determine the possible numbers of NAT sites for each subdistrict based on population distribution and POI data. Then, the P-median model is used to generate alternative siting solutions for NAT sites with different numbers. Finally, a bi-objective cost optimisation model considering travel costs and construction costs is proposed, with the Kneedle algorithm used to select the optimal solution. A case study in Shenzhen, China, demonstrates the feasibility and effectiveness of the proposed method at the subdistrict level, with considerations for the daily mobility of residents, and resilient opening of NAT sites for adaptation to population dynamics.

Although the impact of COVID-19 is currently declining, its rapid mutations and repeated outbreaks on a global scale make it still an important threat to the global public health system. Studying the deployment scheme of public NAT services is not only an effective preventive measure for future risks of COVID-19, but also provides a reference for preventing other infectious diseases, and establishing rapid public health responses.

The rest of this paper is organised as follows: Section 2 introduces the study area and datasets used in this study; Section 3 describes the methodology; Section 4 presents and analyzes the results of the case study; and Section 5 concludes this study.

2. Study Area and Data

2.1. Study Area

Shenzhen is one of the largest cities in China, covering an area of 1997.47 km². According to the results of the Seventh National Population Census, the permanent population of Shenzhen was about 17.56 million in 2021, and the average population density is 8791 people per square kilometre [49]. As shown in Figure 1, population density varies significantly across subdistricts. Given the population heterogeneity and large coverage of Shenzhen, selecting it as the study area is beneficial for testing the effectiveness of the proposed method in a challenging context, which can serve as a valuable reference for determining the location scheme of NAT sites in other cities.

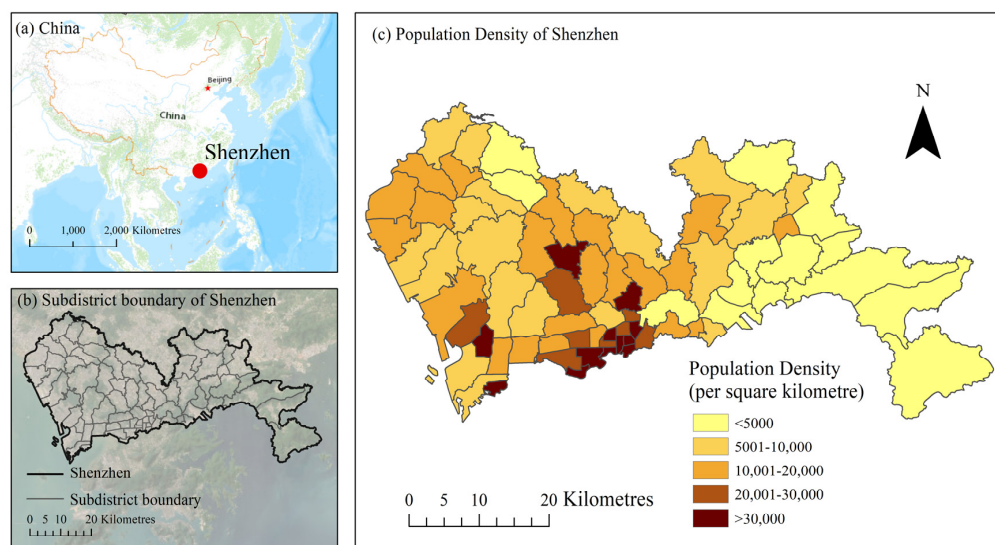


Figure 1. Administrative subdistricts and their population density in Shenzhen.

2.2. Data Collection and Processing

This study retrieved four datasets for solving the location scheme: (1) POIs, (2) road vector data, (3) administrative boundary vector, and (4) population raster in Shenzhen.

- POI data

As discussed in Section 1, public NAT sites are typically located in or near public facilities such as parks, schools, and hospitals. To reduce the potential transmission, NAT sites are also recommended to be set-up in open, well-ventilated spaces. Therefore, we adopted POI data to extract these public facilities as the primary alternatives to NAT sites. POI data in Shenzhen were obtained from the web service provided by Amap API (<https://lbs.amap.com/>, accessed on 15 January 2023). In this study, we retrieved more than 130,000 POIs belonging to six categories, as listed in Table 1.

Table 1. Description of POI data.

ID	Categories	Typical Facilities
1	Scenic spots	Tourist attraction, park square, park, zoo, botanical garden, aquarium, city square, etc.
2	Shopping mall	Store, supermarket, shopping centre, general mall, etc.
3	Transportation facility	Airport, railway station, port terminal, passenger station, etc.
4	Educational and cultural venue	Higher education institutions, secondary schools, elementary schools, museums, etc.
5	Business house	Residential areas, business office buildings, industrial parks, villas, etc.
6	Sports and leisure place	Fitness centre, cinema, KTV, tennis court, gymnasium, etc.
7	Medical institution	Hospital, clinic, health centre, specialised hospital, etc.

- Road vector data

As movable NAT stations are popular in China due to their flexibility, we also added road intersections as a part of the alternatives for placing NAT sites. The road vector data were retrieved from Amap. Compared to other open sources of road data, this road vector dataset presents higher completeness and consistency in China. After topological inspection of the road vector data, we can obtain the error-free road network in Shenzhen. The network is used to extract road intersections which are consequently added to the candidate set.

- Administrative boundary vector

The administrative boundary data were retrieved from the OpenStreetMap project. Considering the central role of the administrative boundary in public health management in China, we took the administrative subdistrict as the basic unit in our siting problem. In that way, the NAT siting problem for Shenzhen would be divided into independent sub-problems for each subdistrict, which would make the results more compatible with the regional characteristics, and promote better management. In this study, we obtained 75 Shenzhen subdistricts (polygons), as shown in Figure 1.

- Population data

Population information of Shenzhen was retrieved from a commercial dataset provided by Merit Interactive Co., Ltd., which was collected on 1 June 2020, through the Software Development Kit (SDK) installed in residents' mobile phones. This SDK dataset provides the population distribution in Shenzhen, with a spatial resolution of 150 m.

As one of the most economically developed cities in China, Shenzhen experiences significant population dynamics, making it crucial to adjust the layout of NAT sites for different periods in order to enhance efficiency and minimize resource waste. Therefore, this study assumes a working period of 8:00 a.m. to 6:00 p.m., and an off-work period of 6:00 p.m. to 8:00 a.m. on the following day. The hourly average population distributions for the two periods are presented in Figure 2. The figure demonstrates that the population distributions during the two periods differ considerably, indicating the necessity of adapting NAT site placement to population dynamics. These distributions were further utilized to showcase the adaptability of our proposed method in addressing such dynamics.

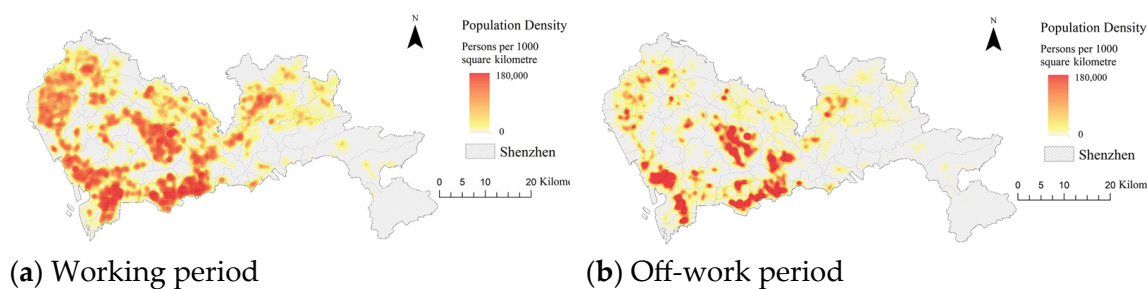


Figure 2. Population density during working and off-work periods.

3. Methods

Figure 3 presents the workflow of our proposed framework for siting NATs, which consists of 3 main steps. Firstly, the number plans of NAT sites are determined using the LSCP model, which generates multiple plans, with varying numbers of NAT sites under coverage constraints and distance thresholds. In the second step, alternative siting plans for NAT sites are determined for each number plan using the P-median model, with a constraint on minimizing the total travel cost. This step aims to improve the distribution of NAT sites for each number plan. Finally, the optimal siting solution is selected using a bi-objective optimization model that balances the construction costs and travel costs.

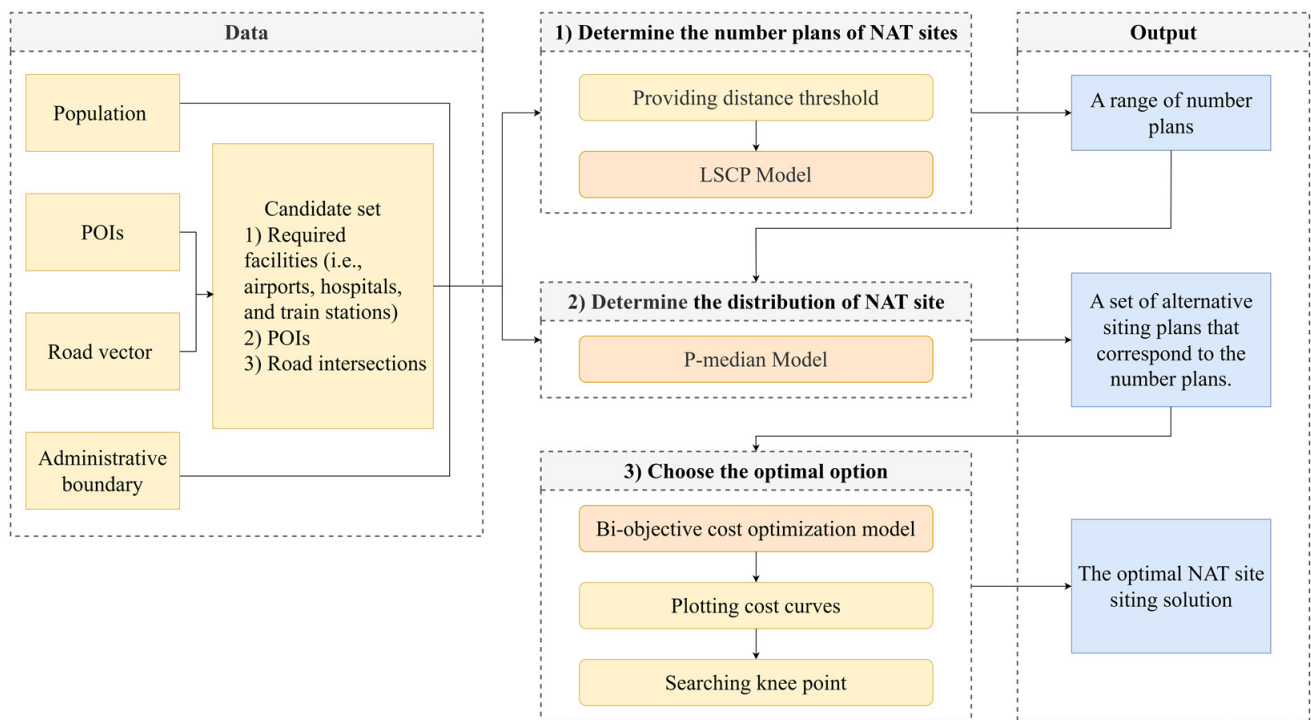


Figure 3. Workflow of the proposed method.

3.1. Determining the Number Plans of NAT Sites

The number of new facilities is critical for solving siting problems. However, the prior number is undetermined in our case. To that end, a distance range $[s_{min}, s_{max}]$ is introduced in this study, to calculate the number range of NAT sites under different distance thresholds. For a given value $s \in [s_{min}, s_{max}]$, we could adopt the LSCP model to determine the minimum number N_s of NAT sites, such that people from any demand point can reach a NAT site along the road network within the distance threshold s . The objective function of the LSCP model could be expressed as [50]:

$$\begin{aligned}
 & \text{Min } \sum_{i \in I} X_i \\
 & \text{s.t. } \sum_{i \in N_i} X_i \geq 1, \text{ all } i \in I \\
 & X_i \in \{0, 1\}
 \end{aligned} \tag{1}$$

The objective function (1) minimises the total number of facilities that would need to be sited in order to cover each and every demand node by at least one facility. I is the set of points where the facilities could be set. When point I is determined as the facility point, X_i is set to 1; otherwise, it is 0.

In this study, the distance range of $[s_{min}, s_{max}]$ was determined by the average walking speed V and predefined time thresholds t_{min} and t_{max} . The speed V was empirically estimated as 1 m/s, whilst t_{min} and t_{max} were set to 5 min and 15 min, respectively. Hence, s_{min} and s_{max} were set to 300 m and 900 m in this study, respectively. It should be noted that, the travel cost was commonly estimated by using the car as the main transportation mode in traditional location-allocation studies. However, in our case, people who seek NAT testing are likely to have been infected, and they are usually encouraged to access nearby NAT sites by walking, in order to reduce the risk of viral transmission. Therefore, we reasonably chose the walking mode, and used 5–15 min as the time interval to evaluate the travel cost, which is also consistent with the “15-min life circle” policy in China.

As a result, we could obtain a range of number plans $Q = \{N | N \in [N_{s_{min}}, N_{s_{max}}], N \in \mathbb{Z}\}$ for planning NAT sites. However, the coverage constraints focused on the ‘reachability’ of NAT sites, while it would underestimate the spatial heterogeneity of the population and the average travel cost made by the residents. Therefore, to reduce the travel cost per capita, we further adapted the P-median model to obtain the distribution of NAT sites under different number plans.

3.2. Determining the Alternative Siting Plans of NAT Sites under Different Number Plans

For a given number plan, we used the P-median model to determine the distribution of NAT sites to minimise the travel cost for all residents within the designated service distance. The objective function of the P-median model is shown as follows [49]:

$$\text{Min} \sum_{i \in I} \sum_{j \in J} a_j d_{ij} Y_{ij}, \quad (2)$$

where I is the set of points where the facilities could be located; J is the set of demand points; a_j is the number of people from demand point j ; and d_{ij} is travel cost from demand point j to facility point i . If demand point j is served by facility i , $Y_{ij} = 1$; otherwise, $Y_{ij} = 0$.

3.3. Choosing the Optimal Siting Solution

After the above step, we can obtain a set of alternative siting plans $W = \{w_N | N \in Q\}$. Intuitively, the number of sites and the travel cost per capital would present a contrary tendency, that is, the average travel cost would decrease with the increment of site number, and vice versa. To balance the travel cost and site number, a bi-objective optimisation model based on travel cost and construction cost is introduced in this study.

The optimal solution is expected to reduce, as much as possible, the costs of residents’ travelling to access NAT sites, and their construction costs. For the travel costs, we considered the time it took for the population to reach the nearest NAT site, and proceed to describe it by the following equation:

$$\text{Min} S_T = \sum_{i \in I} \sum_{j \in J} P_j \times \frac{D_{ij}}{v} \quad (3)$$

$$\text{Min} S_C = \sum_{i \in I} \left(a \times \frac{H_i}{b} + f \right) \quad (4)$$

where the cost of expression (4) includes total medical staff expenditure and fixed total construction expenditure, and a , b and f are three constants— a is the expenditure for medical staff, b refers to the number of patients that one medical staff can treat, and f indicates the basic cost of setting up a NAT site. The number of medical staff at site i is estimated by dividing the number of people covered by the site’s service area H_i by b . In this study, we set $a = 1000$, $b = 360$, and $f = 2000$, which are determined according to the relevant regulations issued by the Chinese government [51,52].

Figure 4 shows the cost curve under time thresholds. It can be seen that the curve is a convex curve. Consequently, we used the python package Kneed [44] to find the knee point on the curve, which corresponds to the optimal solution in this study.

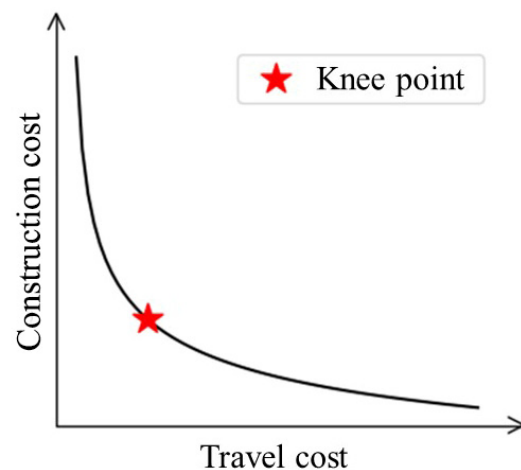


Figure 4. Geometric expression of the knee point.

4. Results

4.1. Example of the Determination of Siting Plans at the Subdistrict Level

We took the subdistrict of Nanyuan as an example to demonstrate the outcomes of each step in our proposed method. As shown in Figure 5, Nanyuan is a typical subdistrict with a dense and heterogeneous population. Significant population dynamics can be observed in Nanyuan during the working and off-work periods of the day. These properties of Nanyuan make it suitable to demonstrate the adaptability of our method.

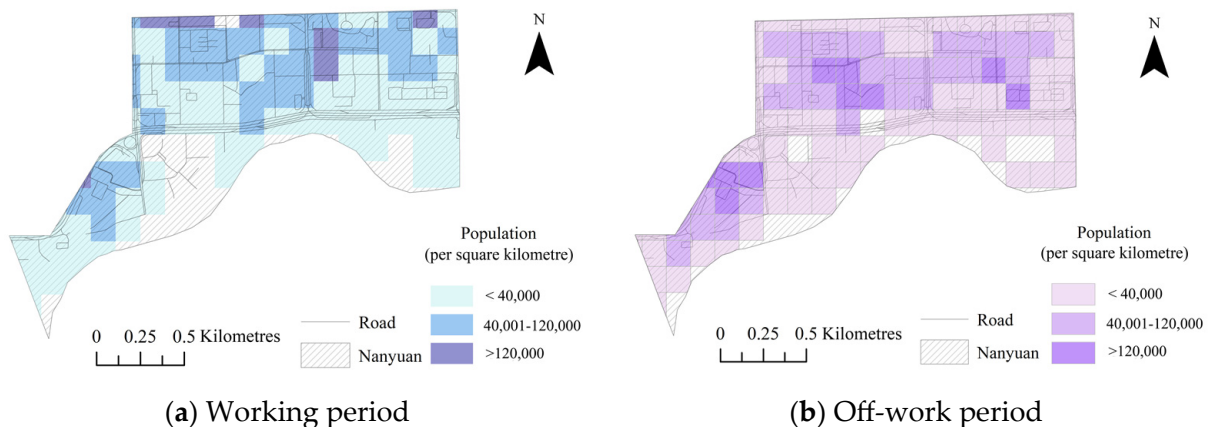


Figure 5. Population distribution of Nanyuan.

For simplicity, in this subsection we focus on the siting plans in Nanyuan during the working period. Using the Location-Allocation tool in the Network Analysis module integrated within ArcGIS 10.7, the LSCP and P-median models were applied sequentially to the Nanyuan subdistrict. Within the given interval of walking distance (i.e., 300 m to 900 m), we could obtain 17 alternative siting plans of Nanyuan, in which the number of sites ranged from 6 to 22. The distribution of the NAT sites under each plan is plotted in Figure 6. It can be seen that, with the increment of N , more sites tend to be placed, which resulted in lower average travel costs for residents, but higher construction costs.

Accordingly, the curve between travel cost and construction cost is depicted in Figure 7. It is generally a convex curve, which could satisfy the premise for using the Kneedle algorithm. Finally, we selected the alternative siting plan with $N = 7$ corresponding to Figure 6b based on the Kneedle algorithm.

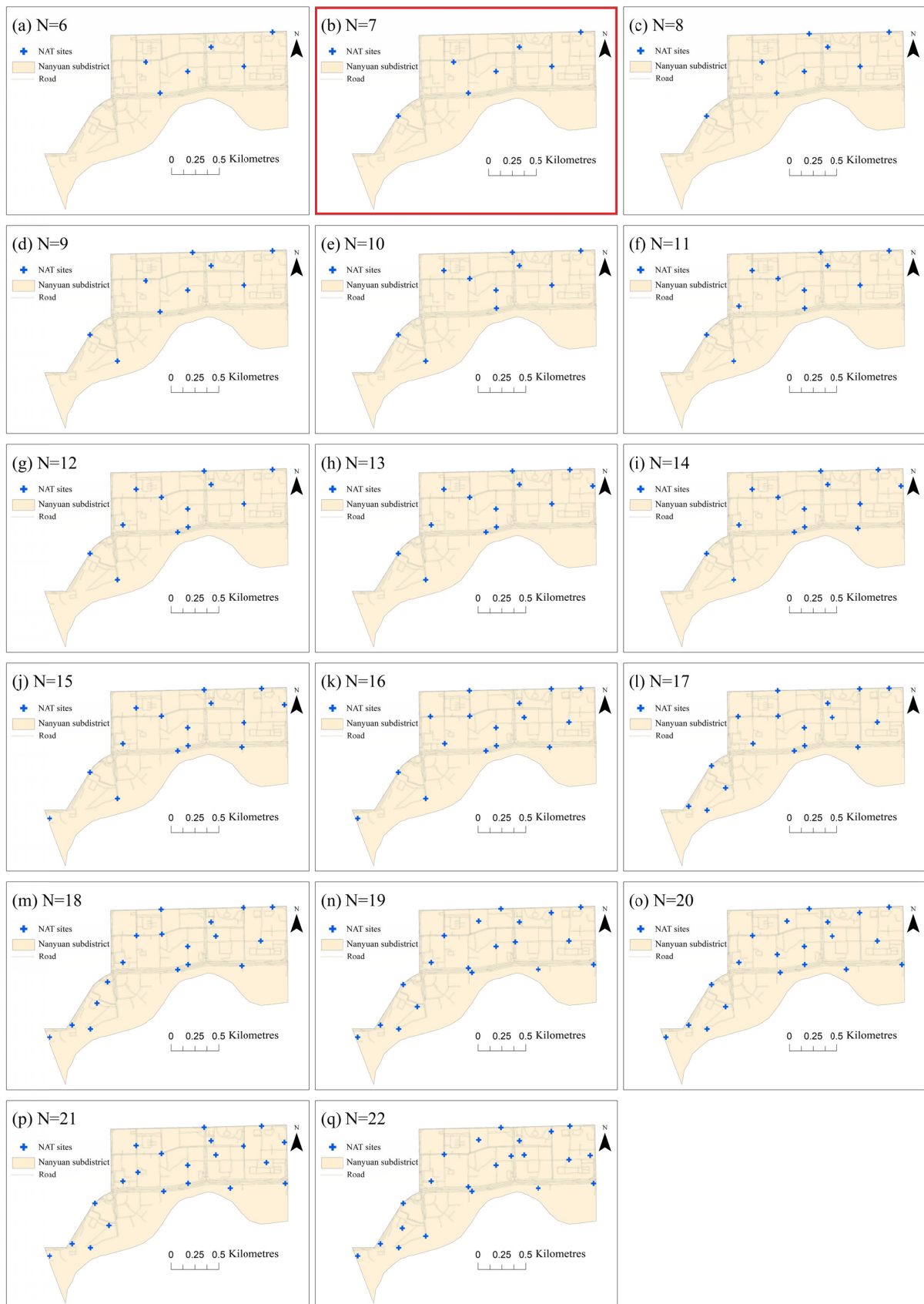


Figure 6. Alternative siting plans of NAT sites under different values of N .

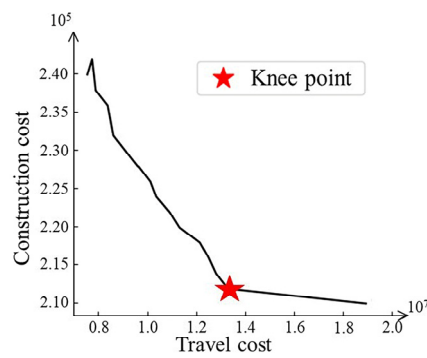


Figure 7. Geometric expression of the knee point of Nanyuan.

4.2. Comparison of NAT Sites in Two Time Periods

Following the same steps described in Section 4.1, we further obtained the optimal siting solution for the off-work period in Nanyuan. The distribution of NAT sites during 2 periods is compared in Figure 8. It can be found that the spatial layout of siting solutions has a strong connection with population density. The optimal plan for the working period sets fewer NAT sites than that during the off-work period. This could be explained by people being clustered in workplaces, so setting fewer sites at the centre of people’s workplaces would be sufficient. However, as the population disperses after work, more NAT sites are required in order to accommodate people in remote regions.

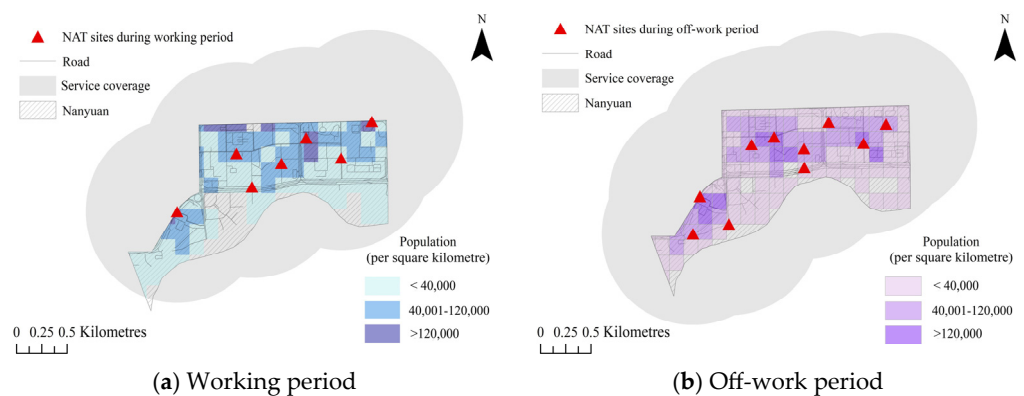


Figure 8. Service coverage of Nanyuan subdistrict.

We further extended the experiments to the whole city, and the statistical results are listed in Table 2. It can be seen that the NAT siting solutions for both time periods have superior population coverage for the population in their respective time periods, and both are above 99%, indicating that it is required and appropriate to plan the NAT sites during two time periods.

Table 2. Population coverage of Shenzhen.

Plan	Population Coverage (%)	
	Working Period	Off-Work Period
Optimal plan for working period	99.53	98.75
Optimal plan for off-work period	99.63	99.48

As shown in Figure 9, most subdistricts have a close number of NAT sites during working and off-work periods. However, there are a few subdistricts that have a higher number of NAT sites during the off-work period than during the working period. For example, the Baolong subdistrict (ID = 2) is intended to be a high-tech industrial gathering centre, and the land is mostly used for industrial production. Figure 9 demonstrates that

there are 78 NAT sites in Baolong during the working period, and only 64 during the off-work period. On the contrary, the subdistrict Longcheng (ID = 33) has a resident population of roughly 500,000. During the off-work period, there are 10 more NAT sites than there are during the working period.

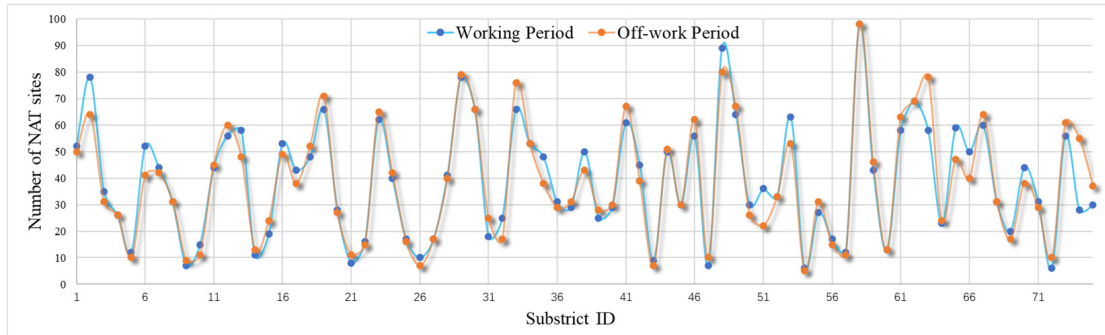


Figure 9. Comparison of the number of NAT sites in different regions and periods.

4.3. Performance Analysis in Regions with Varying Population Amount

We selected three typical subdistricts in Shenzhen, to further investigate the effectiveness of our method in different population densities and distributions. We chose Lianhua subdistrict as an example of a densely populated region, Dalang subdistrict as an example of a moderately populated region, and Longgang subdistrict as an example of a sparsely populated region. The locations of these 3 subdistricts are shown in Figure 10.

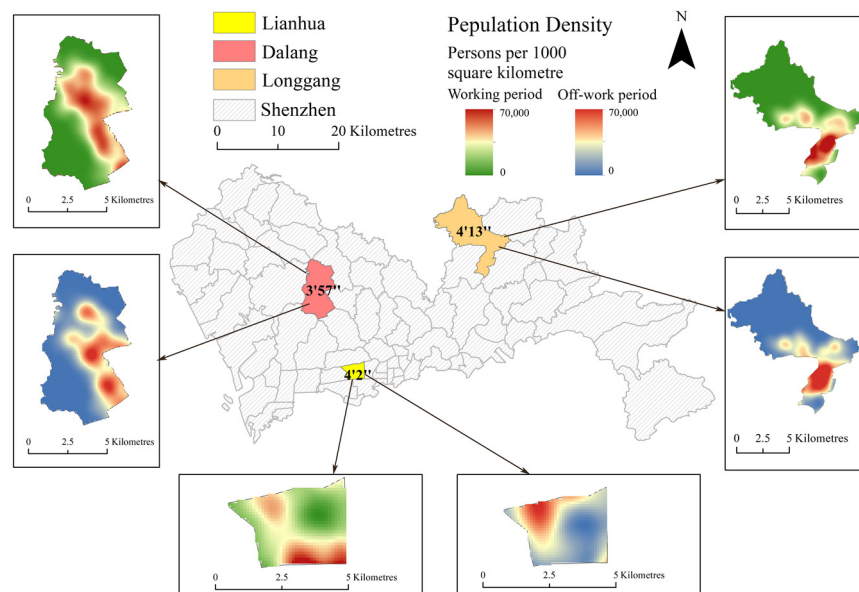


Figure 10. Distribution and population dynamics of Lianhua, Dalang, and Longgang subdistrict. The number within the subdistrict indicates the people’s average travel time to reach the nearest NAT site based on our scheme.

Lianhua subdistrict has a balanced distribution of its population, with about 200,000 total residents, and the average time for residents to reach the nearest NAT site is 4 min and 2 s. More than 300,000 people live in Longgang subdistrict, with the majority of them residing in the south, and the average time spent by residents to reach the nearest NAT site is 4 min and 13 s. The population of Dalang subdistrict is linearly distributed along the northwest-southeast trend, with a total population of 400,000, and an average travel time to reach the nearest NAT of, of 3 min and 57 s. Despite the differences in total population and population density, the differences in travel costs between these three subdistricts are almost negligible, which reflects the equity of public health services.

We conducted a further investigation into the Shatoujiao subdistrict (ID = 54), which exhibited the lowest service coverage based on our siting scheme. As detailed in Appendix A, only 86.30% of the population in Shatoujiao is served during the working period, with this number dropping to 79.66% at the end of the working period. In addition, the travel time per person in Shatoujiao is significantly longer compared to other subdistricts. Our investigation has revealed that this reduction in service coverage can be primarily attributed to the unique population distribution and geometry within Shatoujiao subdistrict. As illustrated in Figure 11, the population in Shatoujiao is highly dispersed. Consequently, to minimize the total weighted distance, the P-median model prioritizes placing the facility sites in densely populated areas, and disregards the transportation costs for distant demand points. As a result, the NAT sites in Shatoujiao are unevenly distributed, potentially failing to meet the demand points within the given travel distance tolerance. However, we regard this outcome as reasonable since only a small number of people are outside the scope of the NAT service. Moreover, the increased travel costs for these underserved individuals would result in a reduction in construction costs for the new NAT site.

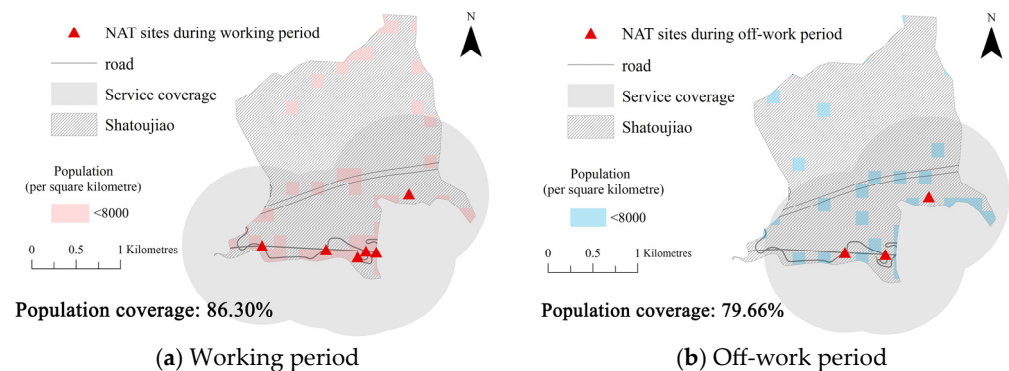


Figure 11. Service coverage of our NAT scheme in Shatoujiao subdistrict.

4.4. Practice with Period Transition and the Relief of Prevention Policy

Through the implementation of our methodology across all subdistricts in Shenzhen, we have generated a comprehensive distribution of NAT sites at the city level. Our calculations reveal that a total of 2919 NAT sites were deployed in Shenzhen during the working period, with service coverage reaching 99.53% of the city's residents. During the off-work period, 2899 NAT sites were deployed, with a maximum service distance of 900 m, effectively covering 99.48% of the population.

To optimize the utilization of resources and accommodate the varying NAT needs of residents, we defined common sites as fixed NAT sites that operate during both working and off-work periods. To identify common sites, we paired NAT sites during working periods with the nearest sites during off-work periods, provided that their spatial distance was within 100 m. We then merged each pair by replacing the two sites with the midpoint between them, which we used as the common sites in this study. Through this process, we identified 1475 common sites in Shenzhen. To ensure the resilience of NAT resources, an additional 1444 NAT sites are needed during the working period, and 1431 during the off-work period. The locations of the different types of NAT sites are shown in Figure 12.

4.5. Comparison with the Actual NAT Sites in Shenzhen

With the relaxation of China's current COVID-19 prevention policy, the density of NAT sites deployed will gradually decrease. To aid decision-makers in their decision-making process, we conducted a study on the deployment plan for NAT sites, by examining the average time it takes for residents to reach the closest NAT site after sampling. Table 3 presents the average time required for inhabitants to access the closest NAT site, given the maintenance of 100%, 50%, 25%, and 12.5% of NAT sites in the Lianhua, Longgang, and Dalang subdistricts, respectively. We observed that the average time required increases as the number of reservations declines, while remaining at an acceptable level of approxi-

mately 15 min. Depending on the specific circumstances, city officials can select a proper retention rate to satisfy the decreased demand.

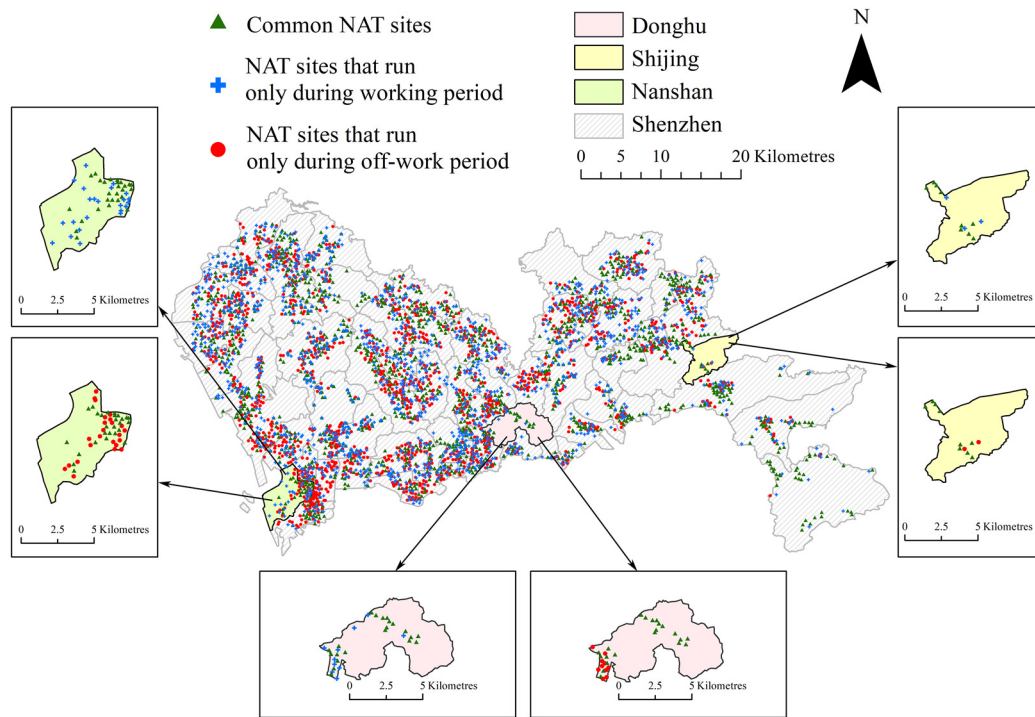


Figure 12. Map of different types of NAT sites in Shenzhen.

Table 3. Data statistics of the population covered by NAT sites service area.

Subdistrict Name	Proportion of Remained NAT Sites (%)	Working Period		Off-Work Period	
		# of NAT Sites	Avg Time (min)	# of NAT Sites	Avg Time (min)
Dalang	100	52	4.64	41	4.05
	50	26	6.35	21	7.11
	25	13	9.83	10	11.56
	12.5	7	14.46	5	17.78
Lianhua	100	18	4.43	25	3.54
	50	9	6.72	13	5.17
	25	5	10.11	6	9.10
	12.5	2	17.77	3	13.05
Longgang	100	53	4.67	53	5.28
	50	27	7.63	27	6.44
	25	13	11.49	13	10.41
	12.5	7	16.63	7	15.80

To study the rationality and applicability of this study, we collected the actual deployment of NAT sites in Shenzhen in November 2022. The Guangming and Pingshan subdistricts were selected to compare the actual scheme to the scheme evaluated by our method. Notably, the full scheme for the rest of the subdistricts in Shenzhen can be found in Appendix A.

Figure 13 shows the spatial distribution and coverage of the actual, and our deployment of, NAT sites, during different periods of the day. The south of Pingshan and the northwest of Guangming were not adequately covered in the actual deployment of NAT sites, and our plan was able to address this issue. As indicated in Table 4, our plan would substantially improve the population coverage of the NAT site deployment plan that was actually implemented. Specifically, under the actual plan, the average time was generally

longer than 15 min, and the population coverage in Guangming was less than 90%, while in Pingshan it was only 76%. In contrast, our plan would reduce the average time to approximately 5 min, and improve the population coverage up to 98% in Guangming and 100% in Pingshan. However, in Pingshan, the number of NAT sites in our scheme differs from that of the actual scheme. To make a fair comparison, we conducted a simulation experiment in which we randomly sampled the same number of NAT sites as in the actual plan, using our solution, multiple times. As shown in the last row in Table 4, our plan, after sampling, could still achieve significantly higher population coverage and lower travel times than did the actual plan used in Pingshan, indicating the superiority of our methods.

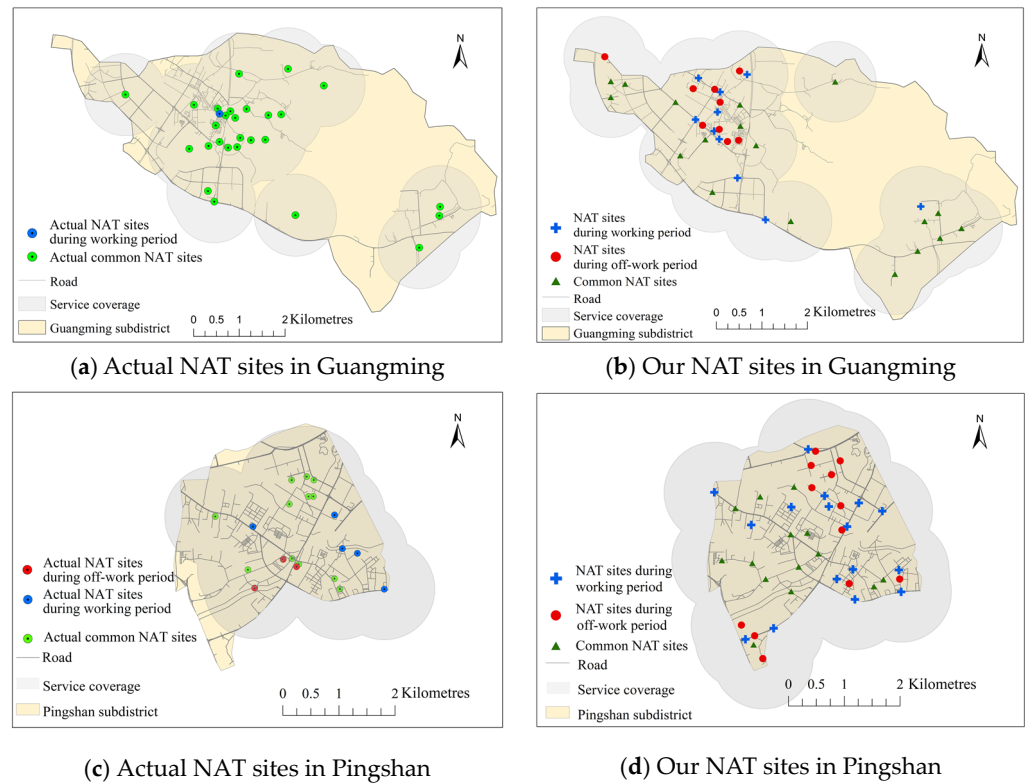


Figure 13. Layout of actual NAT sites, and the NAT sites used in this study.

Table 4. Comparison of the actual scheme and our scheme, in two selected subdistricts.

Subdistrict	Period	# of NAT site		Population Coverage		Average Time to Access (min)	
		Actual	Ours	Actual	Ours	Actual	Ours
Guangming	Working	28	28	81%	98%	9.33	4.97
	Off-work	27	27	88%	99%	8.44	4.21
Pingshan	Working	17	30	76%	100%	9.41	4.26
	Off-work	15	26	76%	100%	8.37	4.21
Pingshan (After sampling)	Working	17	17	76%	97 ± 1.66%	9.41	5.31 ± 0.68
	Off-work	15	15	76%	99 ± 0.12%	8.37	4.37 ± 0.03

5. Conclusions

Epidemic prevention and control constitute a crucial component of public health security. The strategic placement and spatial optimization of NAT (nucleic acid testing) sites are of utmost importance during the fight against COVID-19. In a megacity such as Shenzhen, functional structure and land use differ significantly across different areas, posing formidable challenges for city administrators and healthcare workers alike. With the integration of population and traffic road network data, this study proposed a new analytic framework that adapted the traditional Location-Allocation models and a bi-objective

optimisation model, to plan the city-wide NAT site layout scheme. Our study presents several noteworthy findings based on the case study. Specifically, the results indicate that our proposed scheme, as compared to the existing NAT site arrangement, yields significant improvements in the coverage rate, and in the average time required for NAT testing. At the same time, since our method takes into account the dynamic nature of the population, we have provided a dynamic plan for NAT sites that is adjustive to population distribution, thus reducing the potential redundancy or surplus of medical resources in specific areas.

The framework proposed in this study helps to optimize the spatial allocation of medical resources and provides policymakers with more objective planning guidance, which is essential for effective control of COVID-19 transmission. Although the global epidemic prevention strategy for COVID-19 has recently been relaxed, a wealth of evidence suggests that the potential risk of COVID-19 still exists and threatens the global public health system [53]. The framework is generally applicable to the instant issue on NAT siting and siting of other emergency medical stations, especially when the number of new sites is unknown.

Compared with other methods, the method proposed in this article does not require additional prior knowledge or cumbersome questionnaire surveys. It can directly integrate the population distribution and urban facilities provided by multiple data sources to adaptively formulate the optimal siting plan, improving the efficiency of scheme design, and reducing the uncertainty caused by subjective cognition. At the same time, this method can effectively balance the relationship between the number of selected sites and construction costs, which could be suitable for solving large-scale siting problems under certain conditions, especially where the number of candidate sites is unknown. This characteristic can significantly enhance the usability and robustness of our method in dealing with the complexity and heterogeneity of urban populations, providing new solutions for similar siting problems.

Limitations also exist in this work. Subdistricts were used as the basic processing unit, which aligns with administrative boundaries and allows for a better practical application of our method. However, this operation might introduce some redundant sites at the intersection of different regions. In addition, only travel and construction costs were considered in this study, while many other conditions, such as traffic congestion and waiting time, would also affect the effectiveness of NAT services. Last, but not least, this study assumes homogenous walking speed during the calculation of travel costs to NAT sites, whilst vulnerable populations, such as the elderly and the disabled, might have a higher impedance to access NAT sites, due to their relatively lower mobility. Unfortunately, in the instant study, we cannot distinguish different populations, as our data do not contain personal information. However, once personal information is available, future improvements can be made by increasing the weights of demand points where people are expected to have lower mobility.

Author Contributions: Conceptualization, Siwaner Wang and Qian Sun; methodology, Siwaner Wang.; software, Siwaner Wang and Qian Sun; validation, Pengfei Chen, Yang Chen and Hui Qiu.; formal analysis, Pengfei Chen and Siwaner Wang; investigation, Siwaner Wang; resources, Pengfei Chen; data curation, Pengfei Chen; writing—original draft preparation, Siwaner Wang and Qian Sun; writing—review and editing, Pengfei Chen; visualization, Siwaner Wang and Qian Sun; supervision, Pengfei Chen; project administration, Pengfei Chen; funding acquisition, Pengfei Chen. All authors have read and agreed to the published version of the manuscript.

Funding: This research was funded by the Natural Science Foundation of Guangdong Province (Grant No. 2023A1515011174) and the National Natural Science Foundation of China (Grant No. 42101351).

Data Availability Statement: The POI and road vector data could be retrieved from Amap (<https://lbs.amap.com/>, accessed on 15 January 2023). The administration boundary could be downloaded from the Openstreetmap project (<https://www.openstreetmap.org/>, accessed on 5 January 2023). The population data cannot be publicly shared due to privacy and restrictions from Merit Interactive Co., Ltd.

Conflicts of Interest: The authors declare no conflict of interest.

Appendix A

This appendix includes the number of NAT sites in each subdistrict at different periods, the time it takes to walk to the nearest NAT site per capita, the population coverage of NAT in each subdistrict, and the number of identical NAT sites. The population coverage of NAT in the subdistrict is the percentage of the population in the service area within a 15-min walking radius from the centre of the NAT site outward, to the total population of the subdistrict.

Table A1. Statistics of the NAT site scheme evaluated for each subdistrict in Shenzhen. Subdistricts are labelled by anonymous IDs.

ID	Working Period			Off-work Period			# of Common Sites
	# of NAT Sites	Avg Time (min)	Population Coverage Rate	# of NAT Sites	Avg Time (min)	Population Coverage Rate	
1	52	4.31	99.97%	50	4.5	98.51%	18
2	78	4.56	99.36%	64	4.35	99.65%	27
3	35	4.16	99.57%	31	3.7	99.76%	25
4	26	6.33	96.73%	26	6.27	99.94%	12
5	12	3.14	100.00%	10	5.66	100.00%	3
6	52	4.64	99.71%	41	4.05	99.70%	26
7	44	0.56	95.16%	42	1.09	98.17%	28
8	31	0.59	98.49%	31	1.05	99.16%	21
9	7	4.39	100.00%	9	3.74	100.00%	2
10	15	3.59	100.00%	11	1.4	100.00%	7
11	44	3.77	99.73%	45	3.72	99.90%	31
12	56	3.9	99.59%	60	3.48	99.92%	24
13	58	4.88	99.28%	48	4.52	99.04%	19
14	11	3.88	99.98%	13	3.08	100.00%	4
15	19	5.12	97.84%	24	4.58	100.00%	7
16	53	4.09	99.41%	49	3.81	99.89%	29
17	43	4.04	99.89%	38	3.52	99.91%	24
18	48	4.22	99.90%	52	3.81	99.28%	30
19	66	4.53	99.46%	71	3.95	99.68%	40
20	28	4.97	97.86%	27	4.21	99.12%	18
21	8	4.53	100.00%	11	3.95	100.00%	5
22	16	4.05	99.95%	15	4.1	99.26%	7
23	62	5.16	99.07%	65	4.86	99.43%	35
24	40	4.44	99.60%	42	4.26	98.48%	8
25	17	4.13	99.73%	16	3.64	99.86%	8
26	10	3.33	100.00%	7	4.96	99.99%	4
27	17	4.29	99.36%	17	4.58	99.77%	6
28	41	4.45	99.42%	40	3.86	98.81%	22
29	78	4.79	98.84%	79	4.16	98.14%	40
30	66	4.65	97.86%	66	3.96	98.16%	46
31	18	4.43	99.83%	25	3.54	100.00%	7
32	25	3.63	99.70%	17	4.44	99.81%	10
33	66	5.07	99.30%	76	4.39	99.74%	32
34	53	4.67	99.47%	53	5.28	98.50%	27
35	48	4.68	100.00%	38	5.14	99.36%	20
36	31	3.88	99.88%	29	3.81	99.86%	25
37	29	4.29	98.74%	31	3.26	99.63%	17
38	50	5.02	99.93%	43	4.05	99.03%	17
39	25	4.14	99.84%	28	3.94	99.93%	12
40	29	3.79	98.83%	30	3.15	99.40%	19
41	61	4.3	99.75%	67	4.15	99.93%	26
42	45	0.06	98.35%	39	0.06	98.73%	36
43	9	4.59	100.00%	7	5.67	100.00%	5

Table A1. Cont.

ID	Working Period			Off-work Period			# of Common Sites
	# of NAT Sites	Avg Time (min)	Population Coverage Rate	# of NAT Sites	Avg Time (min)	Population Coverage Rate	
44	50	0.44	98.50%	51	0.55	98.27%	27
45	30	4.01	99.81%	30	4.52	99.85%	11
46	56	4.52	99.25%	62	3.64	99.44%	27
47	7	4.93	100.00%	10	3.38	100.00%	5
48	89	5.07	99.63%	80	4.62	99.65%	36
49	64	5.4	97.17%	67	4.72	98.02%	33
50	30	4.26	99.72%	26	4.21	100.00%	14
51	36	1.33	99.89%	22	2.23	98.55%	21
52	33	4.52	99.51%	33	4.61	98.57%	16
53	63	5.57	99.60%	53	5.57	98.55%	23
54	6	15.74	86.30%	5	35.24	79.66%	3
55	27	4.22	99.18%	31	3.99	99.47%	11
56	17	3.64	99.92%	15	3.61	99.95%	12
57	12	2.65	99.36%	11	2.68	99.20%	9
58	98	6.09	99.02%	98	4.52	99.49%	56
59	43	7.27	97.33%	46	6.02	96.61%	23
60	13	4.08	100.00%	13	3.53	100.00%	5
61	58	1.79	99.76%	63	2.07	99.91%	35
62	69	1.63	98.44%	69	1.37	99.34%	36
63	58	1.6	98.55%	78	1.72	99.51%	30
64	23	3.82	100.00%	24	4.54	100.00%	10
65	59	2.74	99.18%	47	4.22	96.33%	20
66	50	3.55	98.94%	40	4.06	98.51%	27
67	60	4.63	99.77%	64	4.19	99.80%	31
68	31	0.21	99.60%	31	0.27	99.52%	19
69	20	4.34	95.80%	17	7.04	95.47%	11
70	44	4.97	99.06%	38	4.43	98.91%	16
71	31	4.14	99.72%	29	3.53	99.75%	18
72	6	6.14	97.02%	10	4.6	100.00%	2
73	56	4.73	99.71%	61	4.22	99.77%	44
74	28	5.13	98.36%	55	2.76	100.00%	4
75	30	0.12	97.30%	37	0.05	98.21%	11

References

- Fonkwo, P.N. Pricing Infectious Disease: The Economic and Health Implications of Infectious Diseases. *EMBO Rep.* **2008**, *9*, S13–S17. [[CrossRef](#)] [[PubMed](#)]
- Rana, J.S.; Khan, S.S.; Lloyd-Jones, D.M.; Sidney, S. Changes in Mortality in Top 10 Causes of Death from 2011 to 2018. *J. Gen. Intern. Med.* **2021**, *36*, 2517–2518. [[CrossRef](#)] [[PubMed](#)]
- Yin, Y.; Lin, J.; Yuan, S.; Tong, S.; Chen, E.; Zheng, J.; Wang, W. A Booster Shot of Vaccine against SARS-CoV-2 Should Be Rigorously Promoted and Implemented in China. *J. Infect.* **2022**, *86*, e49–e50. [[CrossRef](#)] [[PubMed](#)]
- Lu, J.; du Plessis, L.; Liu, Z.; Hill, V.; Kang, M.; Lin, H.; Sun, J.; François, S.; Kraemer, M.U.; Faria, N.R. Genomic Epidemiology of SARS-CoV-2 in Guangdong Province, China. *Cell* **2020**, *181*, 997–1003. [[CrossRef](#)]
- Siegler, A.J.; Sullivan, P.S.; Sanchez, T.; Lopman, B.; Fahimi, M.; Sailey, C.; Frankel, M.; Rothenberg, R.; Kelley, C.F.; Bradley, H. Protocol for a National Probability Survey Using Home Specimen Collection Methods to Assess Prevalence and Incidence of SARS-CoV-2 Infection and Antibody Response. *Ann. Epidemiol.* **2020**, *49*, 50–60. [[CrossRef](#)]
- Li, Z.; Liu, F.; Cui, J.; Peng, Z.; Chang, Z.; Lai, S.; Chen, Q.; Wang, L.; Gao, G.F.; Feng, Z. Comprehensive Large-Scale Nucleic Acid-Testing Strategies Support China's Sustained Containment of COVID-19. *Nat. Med.* **2021**, *27*, 740–742. [[CrossRef](#)]
- Ali, S.A.; Parvin, F.; Al-Ansari, N.; Pham, Q.B.; Ahmad, A.; Raj, M.S.; Anh, D.T.; Ba, L.H.; Thai, V.N. Sanitary Landfill Site Selection by Integrating AHP and FTOPSIS with GIS: A Case Study of Memari Municipality, India. *Environ. Sci. Pollut. Res.* **2021**, *28*, 7528–7550. [[CrossRef](#)]
- Ajaj, Q.M.; Shareef, M.A.; Jasim, A.T.; Hasan, S.F.; Noori, A.M.; Hassan, N.D. An AHP-Based GIS for a New Hospital Site Selection in the Kirkuk Governorate. In Proceedings of the 2019 2nd International Conference on Electrical, Communication, Computer, Power and Control Engineering (ICECCPCE), Mosul, Iraq, 13–14 February 2019; pp. 176–181.

9. Hashemkhani Zolfani, S.; Yazdani, M.; Ebadi Torkayesh, A.; Derakhti, A. Application of a Gray-Based Decision Support Framework for Location Selection of a Temporary Hospital during COVID-19 Pandemic. *Symmetry* **2020**, *12*, 886. [\[CrossRef\]](#)
10. Harper, P.R.; Shahani, A.; Gallagher, J.; Bowie, C. Planning Health Services with Explicit Geographical Considerations: A Stochastic Location–Allocation Approach. *Omega* **2005**, *33*, 141–152. [\[CrossRef\]](#)
11. Karatas, M. A Dynamic Multi-Objective Location-Allocation Model for Search and Rescue Assets. *Eur. J. Oper. Res.* **2021**, *288*, 620–633. [\[CrossRef\]](#)
12. Devi, Y.; Patra, S.; Singh, S.P. A Location-Allocation Model for Influenza Pandemic Outbreaks: A Case Study in India. *Oper. Manag. Res.* **2021**, *15*, 487–502. [\[CrossRef\]](#)
13. Liu, M.; Xu, X.; Cao, J.; Zhang, D. Integrated Planning for Public Health Emergencies: A Modified Model for Controlling H1N1 Pandemic. *J. Oper. Res. Soc.* **2020**, *71*, 748–761. [\[CrossRef\]](#)
14. He, L.; Xie, Z. Optimization of Urban Shelter Locations Using Bi-Level Multi-Objective Location-Allocation Model. *Int. J. Environ. Res. Public Health* **2022**, *19*, 4401. [\[CrossRef\]](#)
15. Liu, J.; Li, Y.; Li, Y.; Chen, Z.; Lian, X.; Zhang, Y. Location Optimization of Emergency Medical Facilities for Public Health Emergencies in Megacities Based on Genetic Algorithm. *Eng. Constr. Archit. Manag.* **2022**. [\[CrossRef\]](#)
16. Wang, W.; Wu, S.; Wang, S.; Zhen, L.; Qu, X. Emergency Facility Location Problems in Logistics: Status and Perspectives. *Transp. Res. Part E: Logist. Transp. Rev.* **2021**, *154*, 102465. [\[CrossRef\]](#)
17. Celik Turkoglu, D.; Erol Genevois, M. A Comparative Survey of Service Facility Location Problems. *Ann. Oper. Res.* **2020**, *292*, 399–468. [\[CrossRef\]](#)
18. Lei, T.L. Integrating GIS and Location Modeling: A Relational Approach. *Trans. GIS* **2021**, *25*, 1693–1715. [\[CrossRef\]](#)
19. Chen, Y.; Tao, R.; Downs, J. Location Optimization of COVID-19 Vaccination Sites: Case in Hillsborough County, Florida. *Int. J. Environ. Res. Public Health* **2022**, *19*, 12443. [\[CrossRef\]](#)
20. Taiwo, O.J. Maximal Covering Location Problem (MCLP) for the Identification of Potential Optimal COVID-19 Testing Facility Sites in Nigeria. *Afr. Geogr. Rev.* **2021**, *40*, 395–411. [\[CrossRef\]](#)
21. Murray, A.T.; Xu, J.; Wang, Z.; Church, R.L. Commercial GIS Location Analytics: Capabilities and Performance. *Int. J. Geogr. Inf. Sci.* **2019**, *33*, 1106–1130. [\[CrossRef\]](#)
22. Peng, J.; Liu, Y.; Ruan, Z.; Yang, H. *Study on the Optimal Allocation of Public Service Facilities from the Perspective of Living Circle—A Case Study of Xiangyang High-Tech Zone, China*; Research Square: Durham, NC, USA, 2022. [\[CrossRef\]](#)
23. Gomez, D.; Larsen, K.; Burns, B.J.; Dinh, M.; Hsu, J. Optimizing Access and Configuration of Trauma Centre Care in New South Wales. *Injury* **2019**, *50*, 1105–1110. [\[CrossRef\]](#) [\[PubMed\]](#)
24. Kuldeep; Banu, V.; Uniyal, S.; Nagaraja, R. Space Based Inputs for Health Service Development Planning in Rural Areas Using GIS. *Geod. Cartogr.* **2017**, *43*, 28–34.
25. Han, B.; Hu, M.; Wang, J. Site Selection for Pre-Hospital Emergency Stations Based on the Actual Spatiotemporal Demand: A Case Study of Nanjing City, China. *ISPRS Int. J. Geo-Inf.* **2020**, *9*, 559. [\[CrossRef\]](#)
26. Hengel, B.; Causer, L.; Matthews, S.; Smith, K.; Andrewartha, K.; Badman, S.; Spaeth, B.; Tangey, A.; Cunningham, P.; Saha, A. A Decentralised Point-of-Care Testing Model to Address Inequities in the COVID-19 Response. *Lancet Infect. Dis.* **2021**, *21*, e183–e190. [\[CrossRef\]](#) [\[PubMed\]](#)
27. Zhou, X.; Wang, Z. Location Planning of Energy Station Based on P-Median Model. In Proceedings of the Seventh International Conference on Electromechanical Control Technology and Transportation (ICECTT 2022), Dalian, China, 13–15 May 2022; Volume 12302, pp. 1109–1117.
28. Mu, W.; Tong, D. On Solving Large P-Median Problems. *Environ. Plan. B Urban Anal. City Sci.* **2020**, *47*, 981–996. [\[CrossRef\]](#)
29. Grekousis, G.; Liu, Y. Where Will the next Emergency Event Occur? Predicting Ambulance Demand in Emergency Medical Services Using Artificial Intelligence. *Comput. Environ. Urban Syst.* **2019**, *76*, 110–122. [\[CrossRef\]](#)
30. Li, Z.; Xie, C.; Peng, P.; Gao, X.; Wan, Q. Multi-Objective Location-Scale Optimization Model and Solution Methods for Large-Scale Emergency Rescue Resources. *Environ. Sci. Pollut. Res.* **2021**, 1–14. [\[CrossRef\]](#)
31. Fang, Y. Large-scale National Screening for Coronavirus Disease 2019 in China. *J. Med. Virol.* **2020**, *92*, 2266–2268. [\[CrossRef\]](#)
32. Cao, S.; Gan, Y.; Wang, C.; Bachmann, M.; Wei, S.; Gong, J.; Huang, Y.; Wang, T.; Li, L.; Lu, K. Post-Lockdown SARS-CoV-2 Nucleic Acid Screening in Nearly Ten Million Residents of Wuhan, China. *Nat. Commun.* **2020**, *11*, 5917. [\[CrossRef\]](#)
33. Deb, K. Multi-Objective Optimization. In *Search Methodologies*; Springer: Berlin/Heidelberg, Germany, 2014; pp. 403–449.
34. Mishra, S.; Sahu, P.K.; Sarkar, A.K.; Mehran, B.; Sharma, S. Geo-Spatial Site Suitability Analysis for Development of Health Care Units in Rural India: Effects on Habitation Accessibility, Facility Utilization and Zonal Equity in Facility Distribution. *J. Transp. Geogr.* **2019**, *78*, 135–149. [\[CrossRef\]](#)
35. Murray, A.T. Contemporary Optimization Application through Geographic Information Systems. *Omega* **2021**, *99*, 102176. [\[CrossRef\]](#)
36. Ramya, S.; Devadas, V. Integration of GIS, AHP and TOPSIS in Evaluating Suitable Locations for Industrial Development: A Case of Tehri Garhwal District, Uttarakhand, India. *J. Clean. Prod.* **2019**, *238*, 117872. [\[CrossRef\]](#)
37. Firozjaei, M.K.; Nematollahi, O.; Mijani, N.; Shorabeh, S.N.; Firozjaei, H.K.; Toomanian, A. An Integrated GIS-Based Ordered Weighted Averaging Analysis for Solar Energy Evaluation in Iran: Current Conditions and Future Planning. *Renew. Energy* **2019**, *136*, 1130–1146. [\[CrossRef\]](#)

38. Yu, G.; Ma, L.; Jin, Y.; Du, W.; Liu, Q.; Zhang, H. A Survey on Knee-Oriented Multi-Objective Evolutionary Optimization. *IEEE Trans. Evol. Comput.* **2022**, *26*, 1452–1472. [[CrossRef](#)]
39. Zhang, K.; Shen, C.; He, J.; Yen, G.G. Knee Based Multimodal Multi-Objective Evolutionary Algorithm for Decision Making. *Inf. Sci.* **2021**, *544*, 39–55. [[CrossRef](#)]
40. Yu, G.; Jin, Y.; Olhofer, M. Benchmark Problems and Performance Indicators for Search of Knee Points in Multiobjective Optimization. *IEEE Trans. Cybern.* **2019**, *50*, 3531–3544. [[CrossRef](#)]
41. Deb, K.; Gupta, S. Understanding Knee Points in Bicriteria Problems and Their Implications as Preferred Solution Principles. *Eng. Optim.* **2011**, *43*, 1175–1204. [[CrossRef](#)]
42. Das, I. On Characterizing the “Knee” of the Pareto Curve Based on Normal-Boundary Intersection. *Struct. Optim.* **1999**, *18*, 107–115. [[CrossRef](#)]
43. Chiu, W.-Y.; Yen, G.G.; Juan, T.-K. Minimum Manhattan Distance Approach to Multiple Criteria Decision Making in Multiobjective Optimization Problems. *IEEE Trans. Evol. Comput.* **2016**, *20*, 972–985. [[CrossRef](#)]
44. Satopaa, V.; Albrecht, J.; Irwin, D.; Raghavan, B. Finding a “Kneedle” in a Haystack: Detecting Knee Points in System Behavior. In Proceedings of the 2011 31st International Conference on Distributed Computing Systems Workshops, Minneapolis, MN, USA, 20–24 June 2011; pp. 166–171.
45. He, L.; Ishibuchi, H.; Trivedi, A.; Wang, H.; Nan, Y.; Srinivasan, D. A Survey of Normalization Methods in Multiobjective Evolutionary Algorithms. *IEEE Trans. Evol. Comput.* **2021**, *25*, 1028–1048. [[CrossRef](#)]
46. He, Z.; Yen, G.G.; Ding, J. Knee-Based Decision Making and Visualization in Many-Objective Optimization. *IEEE Trans. Evol. Comput.* **2020**, *25*, 292–306. [[CrossRef](#)]
47. Li, K.; Nie, H.; Gao, H.; Yao, X. Posterior Decision Making Based on Decomposition-Driven Knee Point Identification. *IEEE Trans. Evol. Comput.* **2021**, *26*, 1409–1423. [[CrossRef](#)]
48. Branke, J. Consideration of Partial User Preferences in Evolutionary Multiobjective Optimization. *Multiobjective Optim.* **2008**, 157–178. [[CrossRef](#)]
49. Zheng, Z. From the Past to the Future: What We Learn from China’s 2020 Census. *China Popul. Dev. Stud.* **2021**, *5*, 101–106. [[CrossRef](#)]
50. ReVelle, C.S.; Williams, J.C.; Boland, J.J. Counterpart Models in Facility Location Science and Reserve Selection Science. *Environ. Model. Assess.* **2002**, *7*, 71–80. [[CrossRef](#)]
51. Gao, Q.; Shang, W.-P.; Jing, M.-X. Effect of Nucleic Acid Screening Measures on COVID-19 Transmission in Cities of Different Scales and Assessment of Related Testing Resource Demands—Evidence from China. *Int. J. Environ. Res. Public Health* **2022**, *19*, 13343. [[CrossRef](#)]
52. Lyu, Y.; Rong, S.; Sun, F.; Xiang, C.; Li, J. Management of an Emergency Sample Collection Team under the Setting of Whole-Community Severe Acute Respiratory Syndrome Coronavirus 2 Nucleic Acid Testing. *Int. Health* **2022**, *57*. [[CrossRef](#)]
53. Daskalakis, D.; McClung, R.P.; Mena, L.; Mermin, J. Centers for Disease Control and Prevention’s Monkeypox Response Team* Monkeypox: Avoiding the Mistakes of Past Infectious Disease Epidemics. *Ann. Intern. Med.* **2022**, *175*, 1177–1178. [[CrossRef](#)]

Disclaimer/Publisher’s Note: The statements, opinions and data contained in all publications are solely those of the individual author(s) and contributor(s) and not of MDPI and/or the editor(s). MDPI and/or the editor(s) disclaim responsibility for any injury to people or property resulting from any ideas, methods, instructions or products referred to in the content.